

Measurements of near-ultimate strength for multiwalled carbon nanotubes and irradiation-induced crosslinking improvements

BEI PENG^{1†}, MARK LOCASCIO^{1†}, PETER ZAPOL², SHUYOU LI¹, STEVEN L. MIELKE³,
GEORGE C. SCHATZ³ AND HORACIO D. ESPINOSA^{1*}

¹Department of Mechanical Engineering, Northwestern University, 2145 Sheridan Road, Evanston, Illinois 60208-3111, USA

²Materials Science Division, Argonne National Laboratory, 9700 South Cass Avenue, Argonne, Illinois 60439, USA

³Department of Chemistry, Northwestern University, 2145 Sheridan Road, Evanston, Illinois 60208-3113, USA

[†]These authors contributed equally to this work.

*e-mail: espinosa@northwestern.edu

Published online: 10 August 2008; doi:10.1038/nnano.2008.211

The excellent mechanical properties of carbon nanotubes are being exploited in a growing number of applications from ballistic armour to nanoelectronics. However, measurements of these properties have not achieved the values predicted by theory due to a combination of artifacts introduced during sample preparation and inadequate measurements. Here we report multiwalled carbon nanotubes with a mean fracture strength >100 GPa, which exceeds earlier observations by a factor of approximately three. These results are in excellent agreement with quantum-mechanical estimates for nanotubes containing only an occasional vacancy defect, and are ~80% of the values expected for defect-free tubes. This performance is made possible by omitting chemical treatments from the sample preparation process, thus avoiding the formation of defects. High-resolution imaging was used to directly determine the number of fractured shells and the chirality of the outer shell. Electron irradiation at 200 keV for 10, 100 and 1,800 s led to improvements in the maximum sustainable loads by factors of 2.4, 7.9 and 11.6 compared with non-irradiated samples of similar diameter. This effect is attributed to crosslinking between the shells. Computer simulations also illustrate the effects of various irradiation-induced crosslinking defects on load sharing between the shells.

Quantum mechanics calculations^{1–5} predict that defect-free single-walled carbon nanotubes possess Young's modulus values of ~1 TPa, tensile strengths >100 GPa, and failure strains of ~15–30% depending on chirality. However, experimental measurements to date^{6–9}, which have all involved multiwalled carbon nanotubes, have observed markedly lower values for fracture strengths and failure strains. In 2000, a study⁶ reported a mean fracture strength of 28 GPa for outer-shell tensile failure in 19 arc-discharge-grown multiwalled carbon nanotubes, failure strains of between 2 and 13%, and anomalous modulus values as low as 270 GPa. Calculations^{4,10} have suggested that defects introduced by oxidative pitting during nanotube purification can markedly reduce fracture strength. Modelling also indicates that extensive pitting will lead to dramatically lower modulus values and increases in failure strains¹¹.

More recently, fracture studies⁷ on 14 unpurified arc-discharge-grown multiwalled carbon nanotubes yielded a mean modulus value of 955 GPa, in good agreement with theory, but mean fracture strengths and failure strains that were still only 24 GPa and 2.6%, respectively. Potential sources of large defects that might explain the continued underperformance of the measured fracture strengths are the use of sonication to partially disperse

the nanotubes and electron-beam-induced reactions between the nanotubes and residual water in the scanning electron microscope (SEM) chamber, as has recently been observed by Mølhave and colleagues¹². Previous measurements of tensile failure for large-diameter chemical vapour deposition (CVD)-grown multiwalled carbon nanotubes^{8,9} demonstrated multishell failure, frequently involving all shells, at low failure strains. In that work, the number of load-bearing shells was not well characterized, so the fracture strengths were reported as if only a single shell had failed. Under this assumption, the average strength measured for CVD-grown nanotubes was higher than that measured for single-shell fracture of arc-discharge-grown nanotubes, likely due to significant intershell load transfer facilitated by the irregular shell structure (waviness) resulting from the CVD synthesis process. However, if the cross-sectional area of all fractured shells is used in the calculation of the specimen strength, the values would be well below those predicted by theoretical calculations.

Considerable effort has been put into developing methods for purifying nanotubes^{13,14} and for determining the types of defects that are present^{15–17}. The persistent failure of experiments to observe carbon nanotube tensile fracture strengths and strains

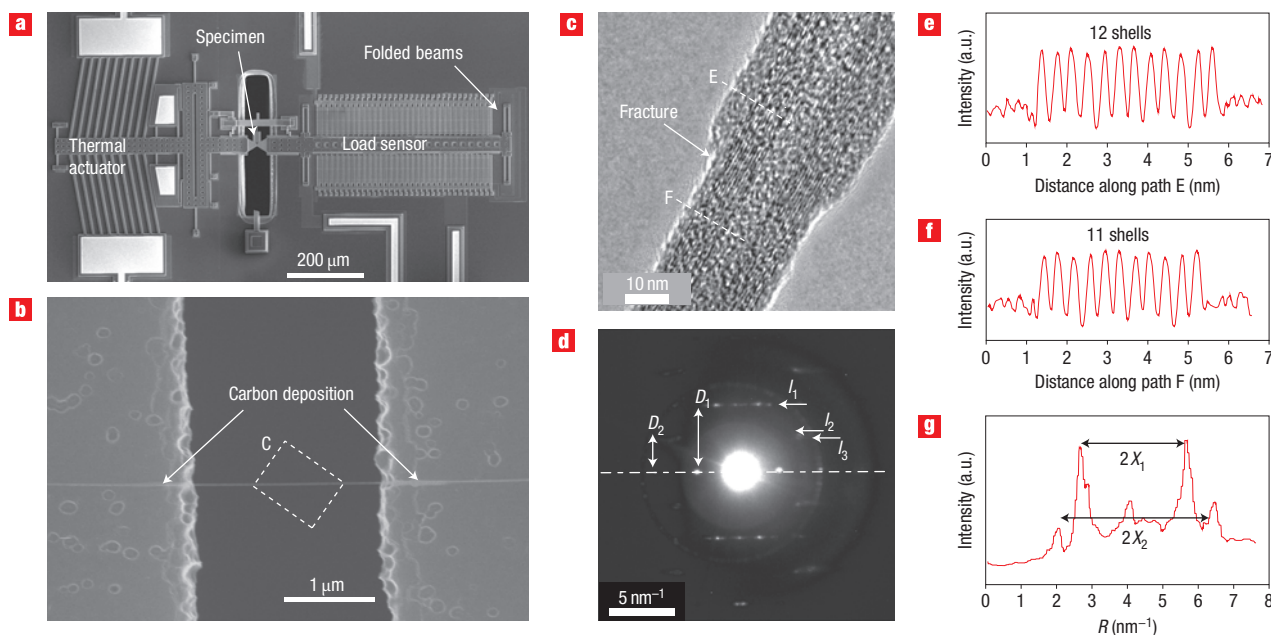


Figure 1 Testing system and *in situ* TEM metrology. **a**, SEM image of the MEMS arrangement used to test the mechanical properties of various carbon nanotubes. **b**, SEM image of a multiwalled nanotube bridging the gap between the actuator (left) and the load sensor. **c**, TEM image of sample 1 after fracture. Paths E and F were used to create intensity profiles on either side of the fracture to verify that only a single shell failed. **d**, Electron diffraction pattern of the nanotube. The principal layer lines are labelled l_1 , l_2 and l_3 , and the layer line spacings are labelled D_1 and D_2 . The dashed line through the centre has been inserted as a reference for D_1 and D_2 , and is not a part of the image. **e**, Intensity profile along path E, showing evidence for 12 shells. **f**, Only 11 shells can be seen in the intensity profile along path F, showing that just one shell failed. **g**, Intensity profile along l_1 . The distances between the peaks are labelled $2X_1$ and $2X_2$.

Table 1 Measured properties for both irradiated and non-irradiated multiwalled carbon nanotubes.

Sample no.	Outer shell chirality	Gauge length (nm)	Outer diameter (nm)	Inner diameter (nm)	No. of broken shells	Total no. of shells	Dose (C cm ⁻²)	Stiffness (N m ⁻¹)	Max load (nN)	Failure stress (GPa)	Modulus (GPa)
1	[184, 8]	1,852	14.72	—	1	12	0	9.6	1,772	98	990
2	[200, 1]	2,024	15.71	—	1	17	0	8.7	1,845	110	1,049
3	—	2,105	25.97	—	1	2 or 3	0	14.6	2,684	97	1,105
4	—	1,035	39.48	37.44	3	18	3.1	114.0	10,326	82	932
5	—	568	25.87	13.69	18	33	31.0	559.4	21,866	58	840
6	—	1,899	49.01	13.47	52	61	558.0	542.1	60,515	35	590

comparable to those predicted by theory has also led to speculation that, even in perfect samples, aggregation¹⁸ of stress-induced¹⁹ Stone–Wales defects²⁰ could lead to failure mechanisms that limit strength.

In this work we present experimental measurements of single-shell failure for multiwalled carbon nanotubes that display fracture strengths of ~ 100 GPa and fracture strains that are very close to theoretical predictions (that is, comparable to what is expected for structures containing only small defects such as vacancies or Stone–Wales defects). We also demonstrate that electron-irradiation-induced crosslinking of multiwalled carbon nanotubes can yield dramatic increases in sustainable loads. Irradiation has already been extensively studied in the context of increasing stiffness^{21–24}, but we show here that although large numbers of defects are introduced in this process, failure strains and failure stresses remain at a significant fraction of what would be expected for non-irradiated shells loaded in tandem. Furthermore, modelling is presented to illustrate the efficiency of load sharing between shells as a function of the type and degree of crosslinking.

TENSILE TESTING: APPROACH AND RESULTS

The experimental work was carried out using an *in situ* transmission electron microscopy (TEM) method using a MEMS material testing system^{25–28} that allows accurate measurement of both load and displacement simultaneously with TEM imaging. Load is applied using a thermal actuator on one side of the mobile testing stage, and displacement is measured using a MEMS differential capacitive sensor on the opposite side (Fig. 1a). Arc-discharge-grown multiwalled carbon nanotubes were mounted on the testing stage using a piezoelectric nanomanipulator built by Klocke Nanotechnik inside a LEO Gemini 1525 SEM. The nanotubes were provided by n-Tec and had a diameter distribution of ~ 2 – 50 nm and an average length of $5 \mu\text{m}$. Scanning electron microscopy images of as-grown (that is, unpurified) multiwalled nanotube powder were used to identify suitable tubes. A selected nanotube was welded to the nanomanipulator probe by electron-beam-induced deposition of carbon and then transported to the MEMS stage and attached by means of carbon deposition at two points. Specimens were

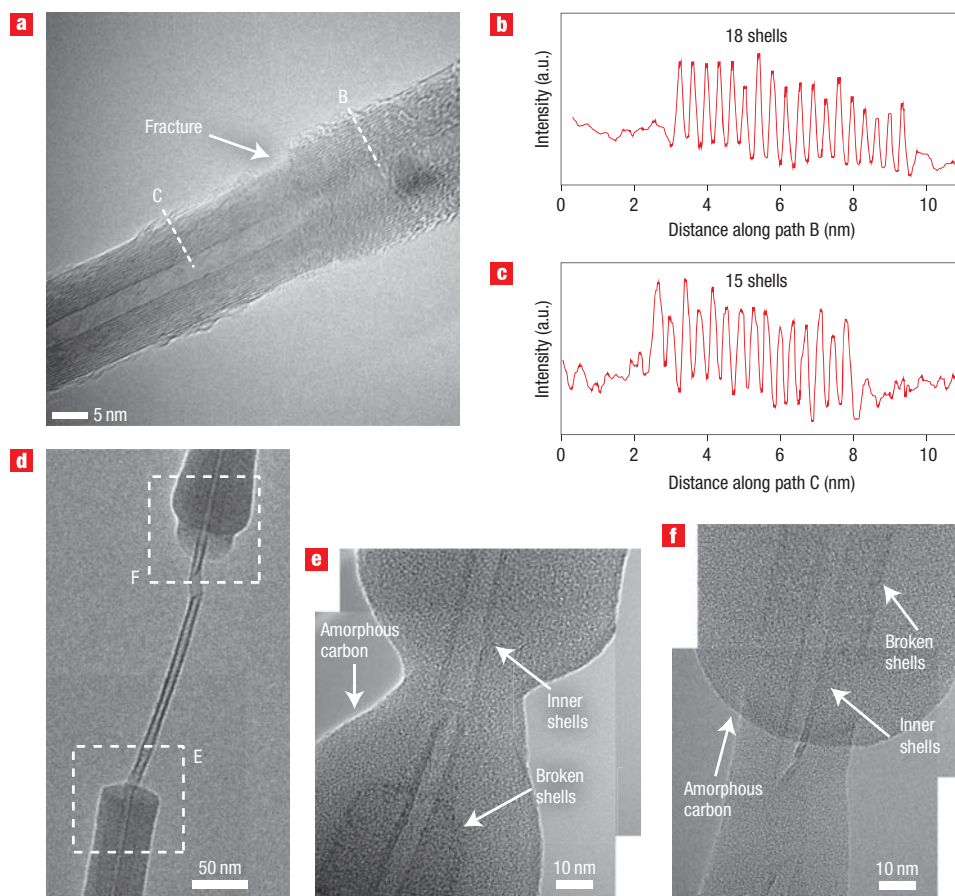


Figure 2 Electron irradiation effects. **a**, TEM image of multiple-shell fracture for sample 4. **b,c**, Paths B (**b**) and C (**c**) were used to create intensity profiles on either side of the fracture to identify the number of failed shells. **d**, TEM image of sample 6. **e,f**, Magnified images of boxes E and F in **d**.

loaded incrementally until failure; the failure regions were then further analysed at high magnifications.

During loading, specimens were imaged using a 100 keV electron beam to minimize the generation of defects, as suggested by earlier work²⁹. Tests of irradiation effects were carried out by focusing the TEM beam on the suspended portion of the tube, and then increasing the beam voltage to 200 kV until the desired dosage was administered. Tensile tests were conducted for three non-irradiated tubes and for three tubes that received varying degrees of irradiation. The geometry, failure load, failure stress, modulus and other properties for these six samples are summarized in Table 1. Note that the gauge lengths—that is, lengths between the fixed points—have the values reported in Table 1. The modulus was found by finite difference in the linear strain regime. Where possible (samples 1–4), the fractured cross-sectional area was defined by the measured diameters and the effective shell thickness of 0.34 nm. At higher irradiation doses (samples 5 and 6) the shell structure could not be clearly identified, so the cross-sectional area was estimated from the configuration of the failed structure observed in the TEM images. Key features are illustrated for a non-irradiated tube in Fig. 1 and for irradiated tubes in Fig. 2. These images reveal one or more fractured outer shells and an inner core that was not load bearing. Note that the amorphous carbon accumulation shown in the images is produced during post-fracture high-magnification TEM imaging and is not present during the loading phase.

Direct observation of the TEM image does not reveal the number of failed shells, but this can be obtained using image-processing techniques. Intensity profiles were taken along two paths, one involving only the inner core and the other involving all shells. These profiles had an improved signal-to-noise ratio that allowed identification of individual shells with the peaks in each profile (Fig. 1e,f and Fig. 2b,c). Fourier analysis of these curves provided a value of 3.4 Å for the mean inter-peak distance, which agrees with values for the interlayer spacing of both multiwalled carbon nanotubes and graphite³⁰. In sample 1, for example, the intensity profiles (Fig. 1e,f) clearly show that only a single shell fractured because there are 12 peaks in the profile of path E and 11 peaks in the profile of path F; similar profiles for sample 4 (Fig. 2b,c) indicate that exactly three shells failed.

For the non-irradiated samples, further analysis of the failed nanotubes was possible using selected area diffraction. The outermost shell dominates the diffraction patterns and this permits determination of the chiral indices [u , v] from the principal layer lines (the bright horizontal lines that appear in the diffraction pattern due to the nanotube's periodic structure) using a procedure outlined previously³¹. The diffraction pattern of sample 1 is displayed in Fig. 1d. The intensity profile of the first principal layer line, I_1 , resembles a Bessel function, the order of which was used to determine the chiral index v . The profile for sample 1 is shown in Fig. 1g. From the measurement, the ratio of the distances between peaks, $X_2/X_1 = 1.47$, gives $v = 8$

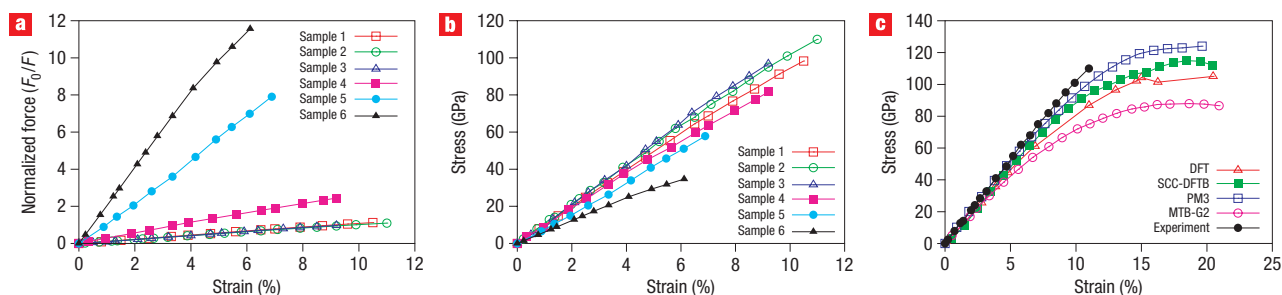


Figure 3 The behaviour of the nanotube samples. **a**, Normalized force versus strain for the six samples tested. The normalizing force F_0 is the product of a nominal failure stress of 100 GPa and the cross-sectional area of the outer shell (so it varies between samples). **b**, Stress versus strain for the same six samples. **c**, Stress–strain curves computed by four different theoretical methods, compared with the experimental measurements for sample 2 (black line). The density functional theory (DFT) and PM3 results are from earlier work⁴.

according to values tabulated previously³¹. The ratio of the chiral indices in terms of the diffraction spacings is given by

$$\frac{v}{u} = \frac{(2D_2 - D_1)}{(2D_1 - D_2)}, \quad (1)$$

which specifies the value of u , given v , D_1 and D_2 (Fig. 1d). The diameter of the nanotube was then computed from its indices using the formula

$$D = \frac{2.46 \text{ \AA} \sqrt{u^2 + v^2 + uv}}{\pi}. \quad (2)$$

The experimental results indicate that the outer shell of sample 1 is a [184, 8] nanotube and the outer shell of sample 2 is a [200, 1] nanotube; a determination was not possible for the third sample.

Normalized force–elongation and nominal stress–nominal strain curves computed from the measured force–displacement data are displayed in Fig. 3a,b, respectively. The initial unstressed diameter was used to compute nominal stresses. For the three non-irradiated samples, very similar stress–strain curves were obtained, with single-shell failure observed in each case.

As a result of variations in the tested specimens' length and diameter, normalized loads and elongations were used for comparing the performance of the six tubes (Fig. 3a). The load was normalized by a force F_0 defined as the product of the outer shell cross-section and a nominal failure stress of 100 GPa. Elongations were normalized by the original gauge length.

Figure 3c compares the stress–strain curve for sample 2, which is nearly zigzag in chirality, to theoretical stress–strain curves for a [10, 0] zigzag single-walled nanotube. The computed curves include previously reported results⁴ using density functional theory, the semi-empirical quantum-mechanical model PM3³², and the empirical second-generation modified Tersoff–Brenner (MTB-G2) potential^{33,34}, as well as new results using self-consistent charge density functional-based (SCC-DFTB) tight binding³⁵. The modified Tersoff–Brenner displays a more compliant response than the quantum mechanics models, which is particularly noticeable at higher strains, but this method is sufficient for semiquantitative purposes. The agreement between the experimental curve and each of the quantum mechanics methods is very good, in particular in the case of PM3, with the most noticeable difference arising in the failure strain, which can be rationalized by the presence of small defects. PM3 calculations⁴ indicate that even a single vacancy defect is sufficient to reduce

failure stresses in a [10, 0] tube from 124 to 101 GPa and to reduce failure strains from ~20% to ~13%. Additionally, the short tube lengths used in the defected tube quantum mechanics calculations tend to slightly overestimate failure strains. Even the most meticulous synthetic processes may be expected to produce carbon nanotubes with an occasional vacancy defect. Thus, the experimental measurements reported here are entirely consistent with the maximum anticipated properties of carbon nanotubes and the fracture strength is within ~20% of the ultimate strength of hypothetical perfect tubes.

As seen in Fig. 3a,b, the stiffness and fracture characteristics of the irradiated tubes changed radically due to an increase in the number of failing shells. The sample with the lowest irradiation dose (sample 4) fractured in a similar manner to sample 1, except that the three outermost shells failed simultaneously. The higher irradiation doses used for samples 5 and 6 led to approximately 18 and 52 shells, respectively, bearing load. As the defect density is increased the modulus decreases, with that of samples 5 and 6 being ~840 and ~590 GPa, respectively. Additionally, the failure strain decreases to levels as low as ~6% for the most heavily irradiated sample. Others³⁶ have estimated that the knock-on collision cross-sections for carbon nanotubes irradiated at 200 keV vary from ~3 to 6 barns depending on the incident angle. Using the median of these limits, the estimated number of carbon-atom-knockout collisions in the outer shell for samples 4, 5 and 6, are ~430 (0.0033 defects nm⁻²), ~1,500 (0.033 defects nm⁻²) and ~180,000 (0.60 defects nm⁻²), respectively. The inner core of sample 6 displayed considerable amorphous character (although it is still clearly distinguishable from the coating of purely amorphous carbon produced during high-resolution imaging), whereas the inner cores of samples 4 and 5 retained strong carbon nanotube character. This suggests that the irradiation dosage used in treating sample 6 was well beyond that desired to achieve optimal load bearing.

The three irradiated samples displayed enhancements to their maximum load by factors of ~2.4, ~7.9 and ~11.6, respectively, compared to the expected load they would have borne if only their outermost shell had been loaded. These enhancements are particularly impressive given the number of defects introduced during the irradiation process. Still further enhancements may be possible by refining the impact energy used and the dosage delivered.

ATOMISTIC MODELLING OF INTERSHELL LOAD TRANSFER

Because imaging intershell crosslinks is difficult, we pursued a computational approach to gain further insight into the

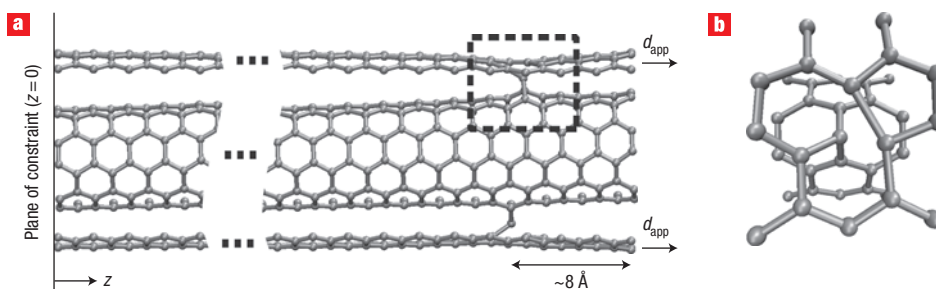


Figure 4 The computational double-walled nanotube model. Atoms in the front and back of the outer shell have been removed for clarity. **a**, Atoms are held fixed in the z -direction on the left ($z = 0$), and displacements are applied only to the outer shell on the right. This mimics the effect of loading only the outer shell, while the inner shell is loaded through the crosslinks only. **b**, A top view of the crosslinking Frenkel pair defect in the dashed box in **a**.

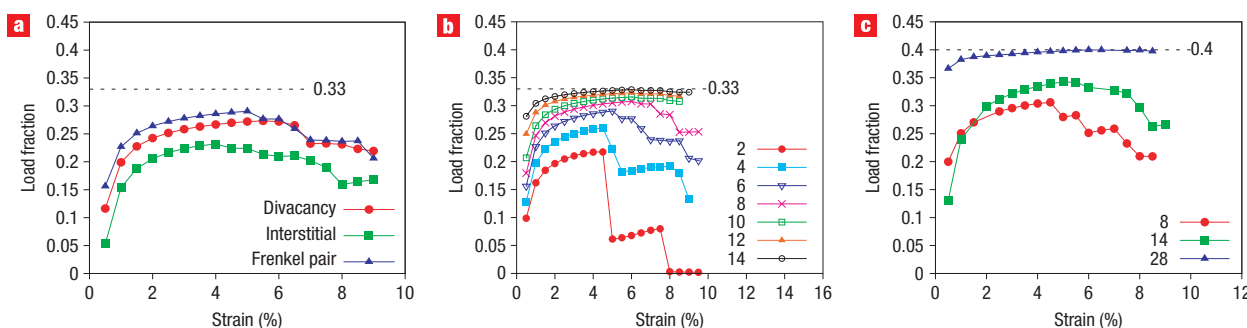


Figure 5 The effects of crosslinking defects on load transfer. **a**, The load fraction on the inner shell versus strain for a $[5, 5]/[10, 10]$ double-walled nanotube containing six Frenkel pair crosslinks (blue), six interstitial crosslinks (green) and six divacancy crosslinks (red). **b**, The load fraction on the inner shell versus strain for a $[5, 5]/[10, 10]$ nanotube containing different numbers of Frenkel pair crosslinks. **c**, The load fraction on the inner shell versus strain for a $[10, 10]/[15, 15]$ nanotube containing different numbers of Frenkel pair crosslinks. The dashed lines in all plots indicate the upper bound for the fraction of the load transferred to the inner shell for that nanotube.

load-transfer mechanism. We used molecular mechanics with a modified second-generation Tersoff–Brenner potential^{33,34}—that is, a reactive empirical bond order potential with the cutoff function removed. A given irradiation dose will determine the defect density (crosslinks) of a multiwalled nanotube based on exposure time and beam energy^{23,37}. As shown in the experimental section, by varying the degree of crosslinking, the mechanical properties of the nanotubes can be tailored. A similar effect was observed for the electrical properties of the nanotubes^{38–40}. Hence, by understanding the effect of intershell crosslinking on the mechanical properties of a multiwalled carbon nanotube, we hope to gain insight into the irradiation dosages necessary to tailor nanotubes to a specific application.

In investigating intershell load transfer, a computational model was chosen consisting of a section of $[5, 5]/[10, 10]$ double-walled carbon nanotube, ~ 72.6 Å long, aligned along the z -direction. The model contained 1,800 atoms and is illustrated in Fig. 4. All atoms for both the inner and outer shell located at $z = 0$ were held fixed in the z -direction, but were free to move in the xy -plane, and at the opposite end a displacement was applied only to the outer shell. The application of constraints to both shells at the left end facilitates the calculation of the load fraction borne by each shell. Initially two defects were placed ~ 8 Å from the loading end and diametrically opposite to each other in order to keep the two shells roughly concentric. Additional defects were added in pairs

at roughly equal distances along the length of the tube to simulate various irradiation doses.

Given that tubes of different diameters exhibit very similar stress–strain behaviour, an upper bound for the load transfer to the inner tube in a double-walled nanotube can be obtained by modelling the system as two parallel springs, where each spring stiffness is proportional to the tube radius. Thus, a $[5, 5]/[10, 10]$ double-walled nanotube would have an inner tube half as stiff as the outer one and, consequently, compatibility and equilibrium provides an upper bound for the fraction of the load transferred to the inner tube of $1/3$. Similarly, the fraction of the load borne by the inner shell of a $[10, 10]/[15, 15]$ double-walled nanotube would have an upper bound of 0.4 .

We first consider the effect of defect type on load transfer. Three primary defect types were investigated: a bridging divacancy defect (analogous to the $V_2(\beta\beta)$ graphitic defect⁴¹), an interstitial defect (that is, a carbon atom inserted between the shells) and a nearest-neighbour Frenkel-pair defect; readers are referred to reference 41 for detailed structural information. Computational curves for these different defects crosslinking the shells of a $[5, 5]/[10, 10]$ double-walled nanotube are shown in Fig. 5a for the case of six crosslinks. The modified Tersoff–Brenner potential predicts that divacancy and Frenkel pair defects transfer load more efficiently than interstitials. The most striking observation, however, is that relatively small numbers of any of the defect

types considered here very effectively transfer load to the inner shell even at high strain values.

We next consider the effect of defect numbers on the load transfer. Figure 5b compares load transfer as a function of strain for various numbers of Frenkel-pair defects in a [5, 5]/[10, 10] nanotube and Fig. 5c considers such load transfers for a [10, 10]/[15, 15] nanotube. At low defect numbers, we observe sequential shear failure of the crosslinks until eventually only the outer shell bears load. At intermediate defect numbers some crosslinks fail, resulting in diminished but significant load transfer that persists up to the failure strain. At defect numbers that are roughly comparable to the number of bonds that would be required to fracture the inner shell, we observe no bridging defect failures and near-optimal load transfer values. At very low strains the load transfer is less than at higher strains. This presumably is due to the initially more compliant nature of the bridging defects compared with the main body of the nanotube shells. However, in longer tubes even a slight deviation between the strain values of the various shells would lead to complete fracture of many bridging bonds, so this effect is not expected on the length-scales present in the current experiments.

The computations confirmed that intershell load transfer improves with increasing defect numbers, as observed in the experimental results. Given the weaker nature of the bonds in the bridging defects as compared to the bond strengths in non-defected regions of the nanotube shells, surprisingly few crosslinks are necessary to achieve optimal load transfer.

CONCLUDING REMARKS

We have resolved a long-standing discrepancy between theory and experiment by providing the first direct measurements for tensile fracture strengths of multiwalled carbon nanotubes that are near the ultimate strength estimates of quantum mechanics calculations. These measurements are the first of their kind in the sense that the number of fractured shells is obtained by direct imaging, thus allowing unambiguous determination of the failure cross-section. We have shown experimentally that electron irradiation leads to multi-shell failure and concomitant dramatic increases in sustainable loads while only modestly decreasing the Young's modulus and failure strains. Computational modelling indicates that relatively small numbers of crosslinking defects lead to near-optimal load transfer. These findings should be of particular value in the scaling up of nanotubes to macroscale ropes and fibres and in the design of electromechanical nanodevices.

Received 12 March 2008; accepted 30 June 2008; published 10 August 2008.

References

- Ogata, S. & Shibutani, Y. Ideal tensile strength and band gap of single-walled carbon nanotubes. *Phys. Rev. B* **68**, 165409 (2003).
- Ozaki, T., Iwasa, Y. & Mitani, T. Stiffness of single-walled carbon nanotubes under large strain. *Phys. Rev. Lett.* **84**, 1712–1715 (2000).
- Dumitrica, T., Belytschko, T. & Yakobson, B. I. Bond-breaking bifurcation states in carbon nanotube fracture. *J. Chem. Phys.* **118**, 9485–9488 (2003).
- Mielke, S. L. *et al.* The role of vacancy defects and holes in the fracture of carbon nanotubes. *Chem. Phys. Lett.* **390**, 413–420 (2004).
- Troya, D., Mielke, S. L. & Schatz, G. C. Carbon nanotube fracture—differences between quantum mechanical mechanisms and those of empirical potentials. *Chem. Phys. Lett.* **382**, 133–141 (2003).
- Yu, M. F. *et al.* Strength and breaking mechanism of multiwalled carbon nanotubes under tensile load. *Science* **287**, 637–640 (2000).
- Ding, W. *et al.* Modulus, fracture strength and brittle vs. plastic response of the outer shell of arc-grown multi-walled carbon nanotubes. *Exp. Mech.* **47**, 25–36 (2007).
- Barber, A. H., Kaplan-Ashiri, I., Cohen, S. R., Tenne, R. & Wagner, H. D. Stochastic strength of nanotubes: An appraisal of available data. *Compos. Sci. Technol.* **65**, 2380–2384 (2005).

- Barber, A. H., Andrews, R., Schadler, L. S. & Wagner, H. D. On the tensile strength distribution of multiwalled carbon nanotubes. *Appl. Phys. Lett.* **87**, 203106 (2005).
- Zhang, S. *et al.* Mechanics of defects in carbon nanotubes: Atomistic and multiscale simulations. *Phys. Rev. B* **71**, 115403 (2005).
- Mielke, S. L. *et al.* The effects of extensive pitting on the mechanical properties of carbon nanotubes. *Chem. Phys. Lett.* **446**, 128–132 (2007).
- Mølhave, K. *et al.* Electron irradiation-induced destruction of carbon nanotubes in electron microscopes. *Ultramicroscopy* **108**, 52–57 (2007).
- Andrews, R., Jacques, D., Qian, D. & Dickey, E. C. Purification and structural annealing of multiwalled carbon nanotubes at graphitization temperatures. *Carbon* **39**, 1681–1687 (2001).
- Haddon, R. C., Sippel, J., Rinzler, A. G. & Papadimitrakopoulos, F. Purification and separation of carbon nanotubes. *MRS Bull.* **29**, 252–259 (2004).
- Mawhinney, D. B. *et al.* Surface defect site density on single walled carbon nanotubes by titration. *Chem. Phys. Lett.* **324**, 213–216 (2000).
- Hashimoto, A., Suenaga, K., Gloter, A., Urita, K. & Iijima, S. Direct evidence for atomic defects in graphene layers. *Nature* **430**, 870–873 (2004).
- Suenaga, K. *et al.* Imaging active topological defects in carbon nanotubes. *Nature Nanotech.* **2**, 358–360 (2007).
- Yakobson, B. I. Mechanical relaxation and 'intramolecular plasticity' in carbon nanotubes. *Appl. Phys. Lett.* **72**, 918–920 (1998).
- Nardelli, M. B., Yakobson, B. I. & Bernholc, J. Mechanism of strain release in carbon nanotubes. *Phys. Rev. B* **57**, R4277–R4280 (1998).
- Stone, A. J. & Wales, D. J. Theoretical-studies of icosahedral C_{60} and some related species. *Chem. Phys. Lett.* **128**, 501–503 (1986).
- Banhart, F. Irradiation effects in carbon nanostructures. *Rep. Prog. Phys.* **62**, 1181–1221 (1999).
- Kis, A. *et al.* Reinforcement of single-walled carbon nanotube bundles by intertube bridging. *Nature Mater.* **3**, 153–157 (2004).
- Sammalkorpi, M., Krashennnikov, A., Kuronen, A., Nordlund, K. & Kaski, K. Mechanical properties of carbon nanotubes with vacancies and related defects. *Phys. Rev. B* **70**, 245416 (2004).
- Huhtala, M. *et al.* Improved mechanical load transfer between shells of multiwalled carbon nanotubes. *Phys. Rev. B* **70**, 045404 (2004).
- Espinosa, H. D., Zhu, Y. & Moldovan, N. Design and operation of a MEMS-based material testing system for *in-situ* electron microscopy testing of nanostructures. *J. Microelectromech. S.* **16**, 1219–1231 (2007).
- Zhu, Y., Moldovan, N. & Espinosa, H. D. A microelectromechanical load sensor for *in situ* electron and X-ray microscopy tensile testing of nanostructures. *Appl. Phys. Lett.* **86**, 013506 (2005).
- Zhu, Y. & Espinosa, H. D. An electromechanical material testing system for *in situ* electron microscopy and applications. *Proc. Natl Acad. Sci. USA* **102**, 14503–14508 (2005).
- Zhu, Y., Corigliano, A. & Espinosa, H. D. A thermal actuator for nanoscale *in-situ* microscopy testing: Design and characterization. *J. Micromech. Microeng.* **16**, 242–253 (2006).
- Smith, B. W. & Luzzi, D. E. Electron irradiation effects in single wall carbon nanotubes. *J. Appl. Phys.* **90**, 3509–3515 (2001).
- Endo, M. *et al.* Stacking nature of graphene layers in carbon nanotubes and nanofibres. *J. Phys. Chem. Solids* **58**, 1707–1712 (1997).
- Qin, L.-C. Electron diffraction from carbon nanotubes. *Rep. Prog. Phys.* **69**, 2761–2821 (2006).
- Stewart, J. J. P. Optimization of parameters for semi-empirical methods. I. Method. *J. Comp. Chem.* **10**, 209–220 (1989).
- Brenner, D. W. *et al.* A second-generation reactive empirical bond order (REBO) potential energy expression for hydrocarbons. *J. Phys. Condens. Matter* **14**, 783–802 (2002).
- Shenderova, O. A., Brenner, D. W., Omelchenko, A., Su, X. & Yang, L. H. Atomistic modelling of the fracture of polycrystalline diamond. *Phys. Rev. B* **61**, 3877–3888 (2000).
- Elstner, M. *et al.* Self-consistent-charge density-functional tight-binding method for simulations of complex materials properties. *Phys. Rev. B* **58**, 7260–7268 (1998).
- Zobelli, A., Gloter, A., Ewels, C. P., Seifert, G. & Colliex, C. Electron knock-on cross-section of carbon and boron nitride nanotubes. *Phys. Rev. B* **75**, 245402 (2007).
- Krashennnikov, A. V., Nordlund, K., Sirvio, M., Salonen, E. & Keinonen, J. Formation of ion-irradiation-induced atomic-scale defects on walls of carbon nanotubes. *Phys. Rev. B* **63**, 245405 (2001).
- Gomez-Navarro, C. *et al.* Tuning the conductance of single-walled carbon nanotubes by ion irradiation in the Anderson localization regime. *Nature Mater.* **4**, 534–539 (2005).
- Bockrath, M. *et al.* Resonant electron scattering by defects in single-walled carbon nanotubes. *Science* **291**, 283–285 (2001).
- Charlier, J.-C., Blase, X. & Roche, S. Electronic and transport properties of nanotubes. *Rev. Mod. Phys.* **79**, 677–732 (2007).
- Telling, R. H., Ewels, C. P., El Barbary, A. A. & Heggge, M. I. Wigner defects bridge the graphite gap. *Nature Mater.* **2**, 333–337 (2003).

Acknowledgements

Financial support for this work was provided by the National Science Foundation (CMMI 0555734 and CHE-0550497) and the Office of Naval Research (N000140710905 and N000140810108). The tests were performed at the Electron Probe Instrumentation Centre (EPIC) at Northwestern University. The authors thank I. Petrov and E. Olson for their contribution in the development of the *in situ* TEM holder. G.C.S. and S.L.M. acknowledge the NASA University Research, Engineering and Technology Institute on Bio Inspired Materials (NCC-1-02037). P.Z., and use of the Centre for Nanoscale Materials at Argonne National Laboratory, were supported by the Department of Energy (DE-AC02-06CH11357).

Author contributions

H.E. conceived and designed the experiments. B.P. and S.L. performed the experiments. H.E., P.Z., G.S. and M.L. conceived the simulations. All authors analysed the data. S.M. contributed analysis tools. All authors discussed the results and co-wrote and commented on the manuscript. B.P. and M.L. contributed equally to this work.

Author information

Reprints and permission information is available online at <http://npg.nature.com/reprintsandpermissions/>. Correspondence and requests for materials should be addressed to H.D.E.